J Korean Med Sci 2008; 23: 691-9
ISSN 1011-8934
DOI: 10.3346/jkms.2008.23.4.691

Experimental Pulmonary Fat Embolism: Computed Tomography and Pathologic Findings of the Sequential Changes

This study was done to demonstrate the computed tomography (CT) and pathologic findings of the sequential changes for experimental pulmonary fat embolism (PFE), and to correlate the CT and pathologic findings of rabbit lung. PFE was induced by an intravenous injection of 0.2 mL linoleic acid in 24 rabbits. The rabbits were divided into 4 groups of 6 rabbits each. CT scans were obtained sequentially at 2 hr (n=24), day 1 (n=18), day 3 (n=12) and day 7 (n=6) after fat embolization. The pathologic findings were analyzed and CT-pathologic correlation was done. CT scans showed bilateral ground-glass opacity (GGO), consolidation and nodule in all cases. The findings of PFE at 2 hr after fat embolization were areas of decreased attenuation, GGO, consolidation and nodule. These findings were aggravated on the follow-up CT after 1 day and 3 days. The follow-up CT revealed linear density in the subpleural lungs after 7 days. On CT-pathology correlation, wedge-shaped ischemic necrosis in the subpleural lungs correlated with nodule at 2 hr. GGO and consolidation at day 1 on CT correlated with congestion and edema, and these findings at day 3 were correlated with inflammation and hemorrhagic edema. The linear density in the subpleural lungs correlated with interstitial fibrosis and pleural contraction at day 7. In conclusion, PFE was caused by using linoleic acid which is kind of free fatty acid and this study served as one model of the occurrence of nontraumatic PFE. CT accurately depicted the natural evolution of PFE in the serial follow-up, and this correlated well with the pathologic findings.

Key Words : *Embolism, Experimental Studies; Embolism, Fat; Pulmonary Embolism; Lung, Computed Tomography*

Ok Hee Woo, Hwan Seok Yong, Yu-Whan Oh, Bong Kyung Shin*, Han Kyeom Kim*, and Eun-Young Kang

Departments of Radiology and Pathology*, Korea Lung Tissue Bank, Korea University College of Medicine, Korea University Guro Hospital, Seoul, Korea

Received : 29 August 2007
Accepted : 15 December 2007

Address for correspondence
Eun-Young Kang, M.D.
Department of Radiology, Korea University Guro Hospital, 97 Guro-dong, Guro-gu, Seoul 152-703, Korea
Tel : +82.2-2626-1342, Fax : +82.2-863-9282
E-mail : keyrad@korea.ac.kr

*Supported by a Korea University Grant.

INTRODUCTION

Pulmonary fat embolism (PFE) usually occurs after major trauma-associated long-bone fractures (1); however, it has been only rarely reported in association with a wide variety of nontraumatic conditions, such as diabetes mellitus, burn, infection, neoplasm, sickle cell anemia and total hip or knee replacement (2, 3).

The pathophysiologic mechanism of PFE has been explained by the mechanical and biochemical theories. The mechanical theory postulates that triglyceride particles from the injured adipose tissue enter the circulation and then they obstruct the pulmonary vessels. However, the mechanical theory does not adequately explain the clinical presentation because PFE has been documented to happen in patients suffering with nontraumatic disorders (4). Thus, alternative mechanisms have been suggested. The biochemical theory implicates free fatty acid (FFA), proposing that local hydrolysis of a triglyceride emboli by intrapulmonary lipase, together with the excessive mobilization of FFA from the peripheral adipose tissue by stress hormones, results in toxic pulmonary concentrations of these acids (5). PFE has been suggested to alter the pulmonary hemodynamics and increase the pulmonary vascular permeability in a couple of clinical and experimental models (6, 7).

Experiments on a variety of animal models of acute lung injury by fat embolism with using triolein and FFA have focused on estimating the hemodynamic changes in the pulmonary vasculature (8, 9). However, to the best of our knowledge, few reports have presented descriptions of the radiologic findings, including the computed tomography (CT) findings, of the sequential changes in the experimental PFE models that have used FFA.

In our experimental study, PFE was induced by using linoleic acid, which is a kind of FFA that we used in order to mainly focus on the natural evolution of FFA and the role it plays in nontraumatic PFE. Following this, we analyze the CT and pathologic findings of the sequential changes of the experimental PFE using a FFA, and we correlated this with the CT and pathologic findings of experimentally induced PFE in rabbit lungs.

MATERIALS AND METHODS

Pilot study

Prior to the main experiment, 0.1 mL, 0.2 mL, 0.3 mL, and 0.5 mL of linoleic acid was injected into 5 rabbits, respectively, for the pilot study. The purpose of this pilot study was to test whether linoleic acid could lead PFE or not and to try to know the dose of linoleic acid for tracing to be able to cause acute lung injury. The results on the CT findings showed that after 2 hr, fat embolization could not be observed in the case of the 0.1 mL injection, while the changes on the CT findings after 2 hr of fat embolization were too broad in the cases of the 0.3 mL and 0.5 mL injections, and so these doses of linoleic acid were seemed inappropriate. The CT findings after 2 hr, day 1 and day 3 of fat embolization in the case of the 0.2 mL linoleic acid injection showed various changes for the image findings and the follow-up observations, the same changes as in patients with PFE, while the CT findings after 7 days of fat embolization showed signs of recovery. The observations of the pathologic histology at day 3 and day 7 of the fat embolization in rabbits showed large areas of fat embolism inside the blood vessels and various other pathologic findings. Thus, the 0.2 mL linoleic acid injection was evaluated as being appropriate for the study of the CT findings of PFE induced by FFA.

The animal model and embolization with fat emulsion

All the procedures in this study were conducted under the approval of the animal research committee at the institution where the study was conducted, and the experiments were performed according to the institutional guidelines under sterile conditions at room temperature unless otherwise noted.

Twenty-four adults New Zealand white rabbits that weighed between 3.0 and 3.5 kg each were used for the experiments. All the operations were performed using sterile technique with intramuscular injections of ketamine hydrochloride (Ketalar®; Yuhan Yanghang, Seoul, Korea; 1.0 mL/kg) and xylazine hydrochloride (Rumpun®; Bayer Korea, Seoul, Korea; 0.3 mL/kg).

In 24 rabbits, PFE was induced by intravenous injection through the ear vein with a 1-mL syringe loaded with 0.2 mL dose of linoleic acid (cis-9, cis-12- octadecadienoic acid, 99% purity; Sigma, St. Louis, MO, U.S.A.). After the injection of linoleic acid, 6 mL of normal saline was infused with a 10 mL syringe.

CT scan

Preliminary CTs were performed for all rabbits before the injection of linoleic acid and the CT results were used as the reference data based on which the statements regarding the abnormalities of the lungs were made. To create the models of PFE at different stages, the rabbits were divided into four groups of six rabbits each, and CT scans were then performed: groups I-IV (n=24) underwent CT scans after 2 hr, groups II-IV (n=18) underwent CT scans after 1 day, groups III-IV (n=12) underwent CT scans after 3 days, and group IV (n=6) underwent CT scans after 7 days.

The CT scans were performed with a 16 channel multidetector CT (Somatom sensation 16; Siemens Medical systems, Erlangen, Germany) using 120 mAs, 120 kvP and 0.75 mm collimation. The anesthetic regimen for the CT scan was the same as for the fat embolization. After anesthesia, the rabbits were fixed in the prone position. CT data were constructed using a high-spatial-frequency algorithm and B 60s kernel. The data were reconstructed with a 1.0 mm section thickness for the axial scans and with a 2.0 mm section thickness for the coronal scans with a 12 cm field of view. The scan data were displayed directly on two monitors of a picture archiving and communication system (PACS). Both the mediastinal (window width, 450 HU; window level, 35 HU) and the lung (window width, 1,500 HU; window level, -700 HU) window scans could be viewed.

Analysis of CT images

Two chest radiologists reviewed the CT scans on the PACS by working in consensus. The pattern, distribution and extent of the pulmonary abnormalities were analyzed. The patterns were classified as areas of decreased attenuation, ground-glass opacity (GGO), consolidation, nodule and linear or reticular density. When more than one CT pattern was seen, the predominant pattern and the other CT patterns were described. Areas of decreased attenuation were defined as areas of low density comparing with the adjacent lung tissue. GGO was defined as areas of increased attenuation without obscuration of the underlying vascular markings. Consolidation was considered present when the opacities obscured the underlying vessels. A nodule was considered present when an increased density with a discrete margin was seen. Linear or reticular density was considered present when there was any linear density with an irregular thickness of 1-3 mm was seen.

The anatomic distribution was noted to be peripheral or subpleural if a predominance of abnormality was seen in the outer third of the lung; the anatomic distribution was central if most of the abnormalities were in the inner third of the lung, and the anatomic distribution was peribronchial if a predominance of abnormalities occurred along the bronchovascular bundle and the anatomic distribution was random if no predominance of the abnormalities was observed. The zonal predominance was assessed as upper, lower or diffuse. Upper lung zone predominance was defined as when the abnormalities were above the level of the tracheal carina, and lower zone predominance was defined as when the abnormalities were below that level.

The extent of disease was determined by both observers visu-

ally estimating the percentage of the abnormal lung to the nearest 5% according to each pattern of pulmonary abnormality.

Pathologic examination

After the last follow-up CT scans were performed, each corresponding group of rabbits was sacrificed (e.g. group I after 2 hr, group II after 1 day, group III after 3 days and group IV after 7 days) with an intravenous injection of 6-8 cc of thiopental sodium (Pentothal®; Choong Wae Pharmacy, Seoul, Korea), and the isolated lungs were immediately removed using Radil standard operating procedure for formalin inflation of lungs. Then a radiologist and a pathologist compared the CT results for the axial plane correlated with coronal reconstruction images of upper, mid, lower portion lungs and those for the parts where lung injuries were induced to obtain specimen with dissection. They were then fixed with 10% neutral formalin and embedded in paraffin block. They were cut into 5-μm sections and stained with hematoxylin and eosin (H&E) and oil red O for semiquantification of the fat globules. For the cases showing fat globules, the globules were detected as having distinctive pinkish-red staining.

The pathologic findings were examined by two pathologists with respect to the presence of intravascular or extravascular fat globules, and for the presence and the degree of pulmonary parenchymal changes in comparison with relatively normal lung.

Correlation between the pathologic findings and the CT findings in the same axial plane was determined by two radi-

Table 1. CT findings of sequential changes after fat embolization in rabbit lung

	2 hr (n=24)	1 day (n=18)	3 days (n=12)	7 days (n=6)	*p* value
Ground glass opacity	24 (100%)	17 (94.4%)	11 (91.7%)	1 (16.6%)	0.000
Nodule	16 (66.7%)	13 (72.2%)	9 (75.0%)	1 (16.6%)	0.009
Consolidation	14 (58.3%)	16 (88.9%)	12 (100%)	2 (33.3%)	0.002
Areas of decreased attenuation	6 (25.0%)	2 (11.1%)			0.431
Linear density			3 (25.0%)	6 (100%)	0.009

A change of the incidence of ground glass opacity, consolidation, nodule and linear density was significantly different in the four groups as time progressed (Fisher's exact probability test; $p<0.05$), but areas of decreased attenuation were not significantly different in the four groups.

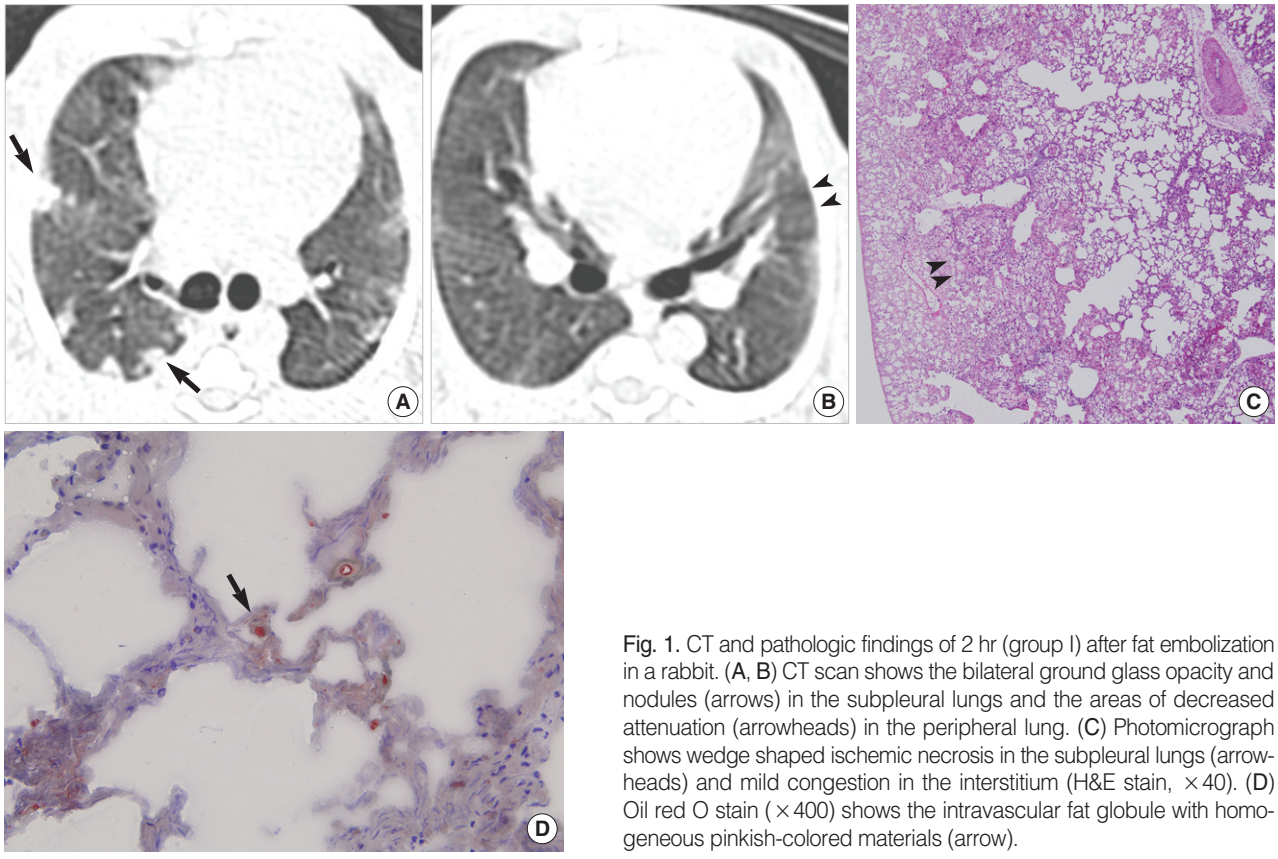

Fig. 1. CT and pathologic findings of 2 hr (group I) after fat embolization in a rabbit. (**A**, **B**) CT scan shows the bilateral ground glass opacity and nodules (arrows) in the subpleural lungs and the areas of decreased attenuation (arrowheads) in the peripheral lung. (**C**) Photomicrograph shows wedge shaped ischemic necrosis in the subpleural lungs (arrowheads) and mild congestion in the interstitium (H&E stain, ×40). (**D**) Oil red O stain (×400) shows the intravascular fat globule with homogeneous pinkish-colored materials (arrow).

ologists and two pathologists all working in consensus.

Statistical analysis

Statistical analysis was performed by using SAS soft ware (SAS Proc Mixed for windows, release 9.1; SAS Institute, Cary, NC, U.S.A.). Differences in the incidence of the CT patterns between the four groups were compared by using Fisher's exact test. Also the differences in the distribution of the CT patterns and disease extent between the four groups were compared by using chi-square test or Fisher's exact test. p values of less than 0.05 were considered to indicate statistically significant differences.

RESULTS

CT findings

The PFE in the rabbits displayed CT and pathologic findings that varied with the passage of time. The CT findings are summarized in Table 1.

At 2 hr after fat embolization in 24 rabbits (Fig. 1A, 2A, 3A, and 4A), GGOs were seen in all 24 cases and consolidations were present in 14 cases. The areas of GGO and consolidation had a subpleural distribution and they had a predominate distribution in the lower part of the lung. Nodules were observed in 16 cases and they were predominate in the upper part of the lung, and they also displayed a subpleural distribution. In 6 cases, the areas of decreased attenuation were seen at the peripheral lungs (Fig. 1B).

At day 1 after fat embolization in 18 rabbits (Fig. 2B), the GGOs were seen in 17 of 18 cases, and consolidations were present in 16 cases. Nodules were observed in 13 of 16 cases. The areas of decreased attenuation were seen in 2 cases.

At day 3 after fat embolization in 12 rabbits (Fig. 3B), GGOs were seen in eleven of 12 cases. Consolidations were present in all 12 cases. Nodules were observed in nine of 12 cases. Linear densities were seen in three of 12 cases and they were predominate in the lower part of the lung, and they had a subpleural distribution.

At day 7 after fat emolization in 6 rabbits (Fig. 4B), GGO and nodule were noted in each 1 case, and consolidations were seen in 2 cases. Linear densities were present in all 6 cases and this had a subpleural distribution. In 3 cases, the linear density had a distribution in the lower part of the lung,

Table 2. Pathologic findings of sequential changes after fat embolization in rabbit lung

	Pathologic findings
2 hr (n=6)	Intravascular fat globule (oil red O staining) Pulmonary vasoconstriction Wedge-shaped ischemic necrosis in the subpleural lungs Mild congestion in the interstitium
Day 1 (n=6)	Intravascular fat globule Infarction in the subpleural lungs Congestion and edema in the interstitium and alveolar space Inflammation in the perivascular space and alveolar wall
Day 3 (n=6)	Extravasation of fat globule into alveolar space or interstitium Distortion and remodeling of vessel wall and intraarterial necrosis Extensive infarction in the subpleural lungs Hemorrhagic edema Extensive inflammation between infarction area and normal lung
Day 7 (n=6)	Histiocytes with ingestion of fat globule No active inflammation and hemorrhagic edema Hyperplasia of type II pneumocyte and multinucleated giant cell Fibrosis of interstitium and pleural contraction

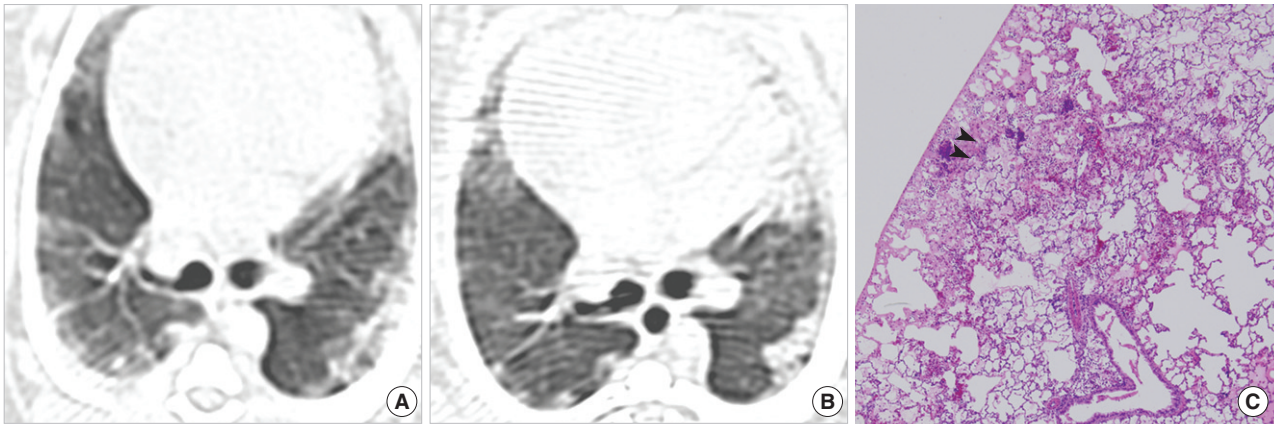

Fig. 2. CT and pathologic findings of sequential changes at 2 hr and day 1 (group II) after embolization in a rabbit. (A) CT scan obtained 2 hr after embolization shows bilateral multifocal ground glass opacities and consolidations. (B) CT scan obtained day 1 after embolization shows more aggravation of the distribution and the extent of the ground glass opacities and consolidations. (C) Photomicrograph shows the more extensive geographic infarction in the subpleural lungs and prominent congestion and edema (arrowheads) in the interstitium (H&E stain, ×40).

while in the three cases, it had a distribution in the upper part of the lung.

A change of the incidence of GGO, consolidation, nodule and linear density was significantly different in the four groups as time progressed (Fisher's exact probability test; $p<0.05$), but the areas of decreased attenuation were not significantly different in the four groups (Table 1). Also a change of the distribution of CT patterns was not significantly different in the four groups.

The extent of the GGO, consolidation and nodule (Fig. 5) gradually increased with time until 3 days, and these findings decreased at day 7. On the contrary, linear density showed its largest extent on day 7. However, a change of the extent of these all findings was not significantly different in the four groups ($p>0.05$).

Histopathologic findings

PFE developed in all twenty-four cases. Sequential pathologic changes were summarized in Table 2.

At 2 hr after fat embolization, pulmonary vasoconstriction in comparison with relatively normal lung and wedge-shaped ischemic necrosis were seen in the subpleural lungs, and mild congestion was seen in the interstitium (Fig. 1C). The vessels were occluded by homogeneous pinkish or red-colored materials that were positive for oil red O stain (Fig. 1D).

At day 1 after fat embolization, congestion and edema in the interstitium were seen, and the infarctions in the subpleural lungs were more severely aggravated than for the findings at 2 hr after fat embolization (Fig. 2C). The perivascular space was infiltrated with inflammatory cells and inflammation of the alveolar wall was noted.

At day 3 after fat embolization, the gross specimen displayed patchy areas of reddish and brownish discoloration on the surface of the subpleural lungs (Fig. 3C). Microscopically, distortion and remodeling of the vessel walls and intraarterial necrosis were visible in the sections stained with H & E. Increasing infarction in the subpleural lungs was observed and hemorrhagic edema was also detected (Fig. 3D). Extensive inflammation between the infarction area and the nor-

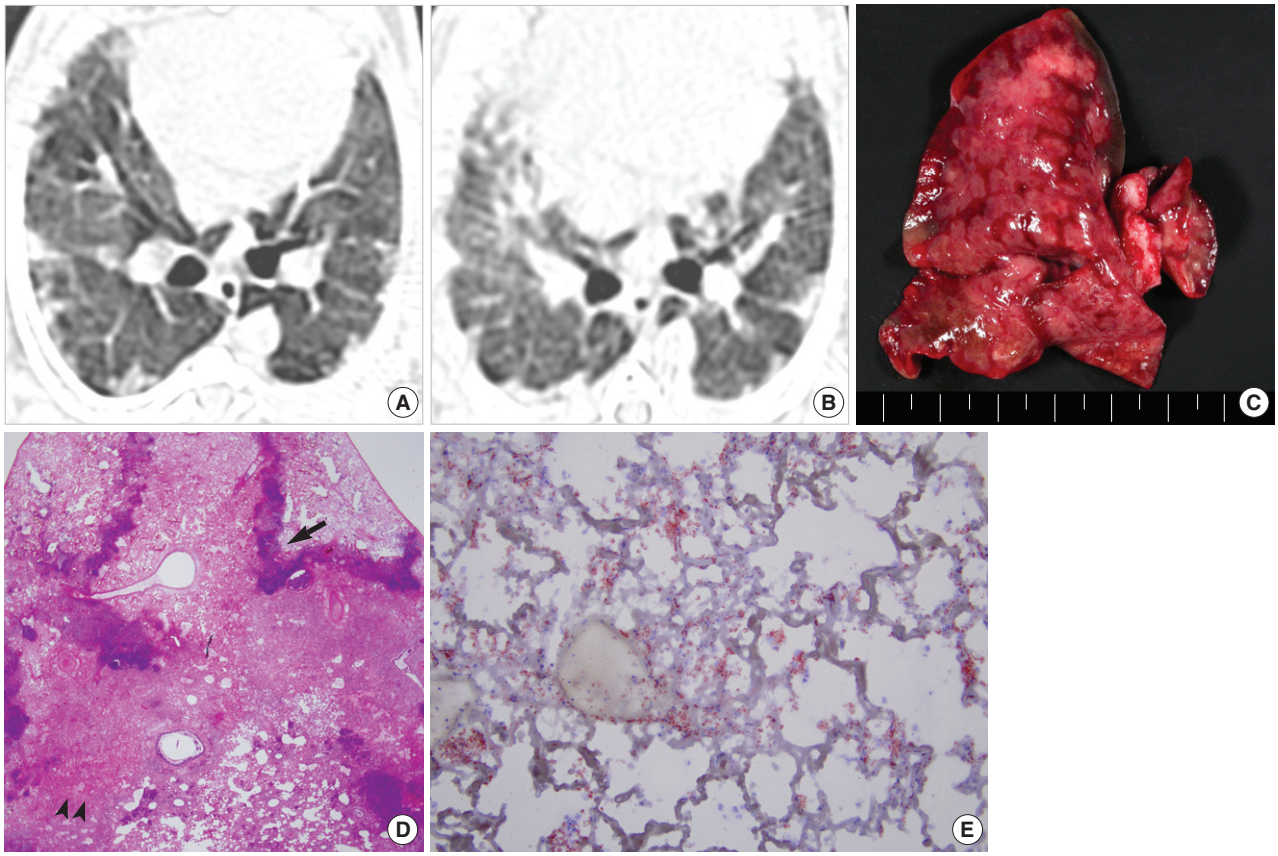

Fig. 3. CT and pathologic findings of sequential changes at 2 hr, day 1 and day 3 (group III) after fat embolization in a rabbit. (A) The CT scan obtained 2 hr after embolization shows GGO, patchy consoliodations and nodules in the subpleural lungs. (B) The CT findings are more extensive and aggravated at day 3. (C) The gross specimen represents the patchy areas of reddish and brownish discoloration of the surface in the subpleural lungs, and this was correlated with the alveolar hemorrhage and inflammation that was seen microscopically. (D) Photomicrograph shows more extensive inflammation (arrow) with hemorrhage and necrosis (arrowheads) in the interstitium (H&E stain, ×40). (E) Oil red O stain (×400) shows extravasated fat globules in the alveolar space or interstitium (arrow) with homogeneous pinkish-colored materials.

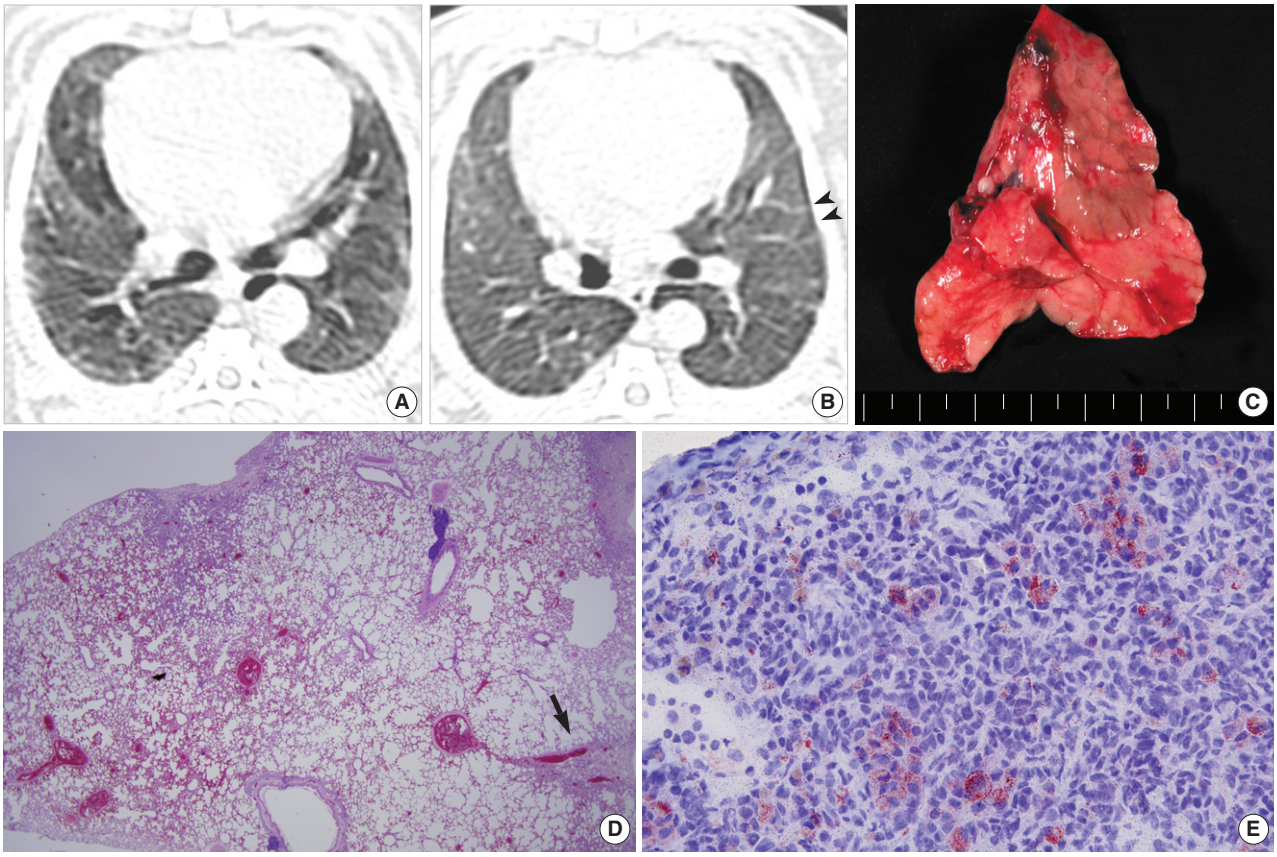

Fig. 4. CT and pathologic findings of sequential changes at 2 hr, day 1, day 3, and day 7 (group IV) after fat embolization in a rabbit. (**A**) The CT scan obtained 2 hr after embolization shows focal GGO at the subpleural lungs. (**B**) The CT scan obtained at day 7 after embolization shows resolution of the parenchymal abnormalities and the linear density (arrowheads) in the subpleural lungs. (**C**) The gross specimen represents the nearly complete resolution of patchy areas of reddish and brownish discoloration of the surface in the subpleural lungs. (**D**) The photomicrograph shows cord-like fibrosis of the interstitium (arrow) and pleural contraction (H&E stain, ×40). (**E**) Oil red O stain (×400) shows histiocytes with ingestion of fat globules.

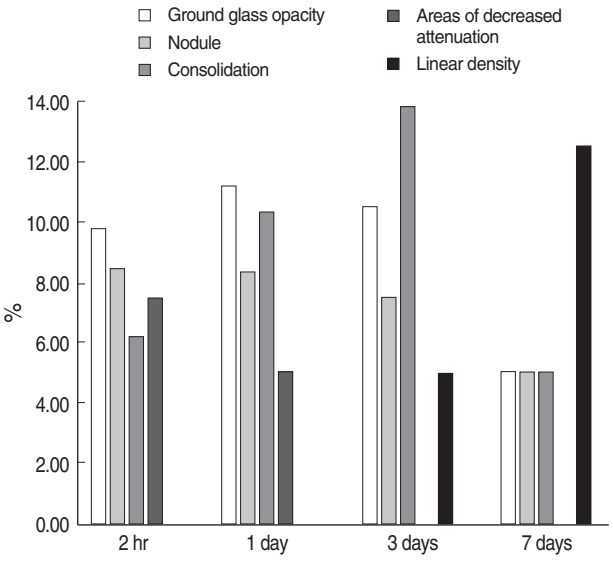

Fig. 5. Extent of parenchymal abnormality on CT scan of sequential changes after fat embolization in rabbit Lung.

mal lung was seen. Extravasation of the fat globules into the alveolar space or the interstitium was present in the sections stained with oil red O (Fig. 3E).

At day 7 after fat embolization, the gross specimens showed resolution of the patchy areas of reddish and brownish discoloration on the surface in the subpleural lungs (Fig. 4C). Microscopically, the active inflammation and hemorrhage had disappeared, but subtle alveolar wall congestion was still seen (Fig. 4D). Also, hyperplasia of the type II pneumocytes and the multinucleated giant cells were visible, and interstitial fibrosis and pleural contraction were revealed. Histiocytes that had ingested fat globules were present in the sections stained with oil red O (Fig. 4E).

CT-histopathologic correlation

The findings on the CT-pathologic correlation are summarized in Table 3.

For the CT-pathology correlation, the corresponding findings were as follows: GGO on the CTs correlated with the

Table 3. CT-pathology correlation of sequential changes after fat embolization in rabbit lung

	CT findings	Pathology findings
2 hr	Areas of decreased attenuation	Pulmonary vasoconstriction Intravascular fat globule (oil red O staining)
	Ground glass opacity	Congestion
	Nodule in the subpleural lungs	Ischemic necrosis
Day 1	Consolidation within ground glass opacity	Congestion and edema
	Nodule in the subpleural lungs	Infarction in the subpleural lungs
Day 3	Consolidation within ground glass opacity or nodule	Extensive accumulation of inflammatory cell Hemorrhagic edema
Day 7	Linear density	Fibrosis of interstitium and pleural contraction

congestion in the interstitium, and the wedge-shaped infarction in the subpleural areas correlated with the nodule seen on the CTs at 2 hr. Also areas of decreased attenuation in the subpleural lungs correlated with pulmonary vasoconstriction at 2 hr. GGO and consolidation on CT at day 1, correlated with the congestion and edema, and these findings on the CTs at day 3 were correlated with the inflammation and the hemorrhagic edema. Linear densities in the subpleural lungs correlated with the interstitial fibrosis and the pleural contraction at day 7.

DISCUSSION

The pathophysiology of PFE is controversial in regards to the origin of the fat droplets that reach the lungs and the mechanism of lung injury from these fat droplets. Many investigators have tried to establish a PFE animal model (6, 10, 11). To date, the tissue damage is believed to be the result of a combination of the mechanical and biochemical effects of the fat (1, 12, 13). Although the debate continues about the pathogenesis of fat embolism, we would agree that PFE is likely caused by the combination of fat deposition in the pulmonary microvasculature and the effects of FFA on the alveolocapillary membrane. Certainly, the occurrence of nontraumatic PFE supports the biochemical mechanism (14). FFAs of an oleic, linoleic, stearic or palmitic acid are normally produced upon the hydrolysis of neutral fat by the lipases that are present in fat deposits. Linoleic acid is an important constituent acid in human fat and the toxicity effect of linoleic acid was thought to the same as the effect in the animal experiments that infused the oleic acid, which was another kind of FFA. Therefore, we induced fat embolization by using linoleic acid, which is a kind of FFA, in order to mainly focus on the natural evolution of FFA in the nontraumatic PFE in our experimental study. The dose of linoleic acid was decided upon by conducting a pilot study, and we also based our decision on the results from the study by Baker et al. (11), in which PFE was induced in dogs by using oleic acid (0.07 mL/kg).

According to Arakawa et al. (15), the CT findings of PFE included areas of consolidation or GGO and nodules in all 6 patients, and these were predominantly found in the upper lobes of the lungs. However, that study did not include the pathologic material for obtaining correlation with the CT findings. In another study reported by Malagari et al. (16), the high-resolution CT findings of mild PFE in nine patients consisted of bilateral GGOs in seven patients and interlobular septal thickenings in five patients. However, the findings in that study were also not proved with a pathologic examination. In our study, PFE was induced by injecting linoleic acid through the intravenous route in all 24 rabbits. The CT findings consisted of bilateral GGOs, consolidation and nodule, and these findings are similar to those described in the previous clinical reports on this condition.

The findings of PFE at 2 hr after fat embolization were areas of decreased attenuation, GGO, consolidation, and nodule with mostly subpleural locations. The pathologic findings at 2 hr after fat embolization were intravascular fat globules. Also, the GGO on the CT were correlated with the congestion in the intersititum. These findings were consistent with the results reported by Derks et al. (17), in which the pathological findings in the lungs of the dogs sacrificed at 1 hr after oleic acid injection were capillary congestion and mild interstitial edema. According to Park et al. (18), the areas of decreased attenuation as an early finding of PFE was observed in most cases, but this was observed only in 25% of the cases of our study. This was considered as being caused by occlusion that was due to capillary embolization, the reduction in the blood circulation due to the pulmonary vasospasm induced by hypoxia, or by the air that was trapped due to bronchospasm.

The GGO, consolidation and nodule were more aggravated on the follow-up CT scan at day 1 and day 3 after fat embolization. The GGO and consolidation on the CT after 1 day, correlated with the congestion and edema, and these findings on the CT after 3 days were correlated with the inflammation and hemorrhagic edema. In particular, hemorrhagic edema was a characteristic finding at day 3, and it is known to be a secondary phenomenon that is due to endothelial vasculitis and leaky vessel syndrome from the toxicity of the FFA (19, 20). In this study, it was directly observed that

the fat globules were seen not only inside the small blood vessels, but they were also seen in the interstitium and alveolar space. Follow-up CT revealed near resolution of GGO, consolidation, and nodule, but linear densities on the subpleural lungs were observed after 7 days. In our experimental study that targeted a rabbit, interstitial fibrosis and pleural contraction at day 7 were observed on the pathologic findings, though this did not exactly match the interlobular septal thickening that is seen in a human. The linear density in the subpleural lungs correlated with the interstitial fibrosis and pleural contraction that was seen on the pathologic findings. This was consistent with the previous reports in which the PFE was improved at between 2 days and 14 days (average: 7 days) (21). In this study, various CT findings were improved after 7 days on the follow-up observation, but adult respiratory distress syndrome can develop in serious cases, according to the literature (3).

Even if there are clinical symptoms of PFE, radiographic changes have been known to appear 2 to 3 days later after the embolic event. On the sequential examinations, the radiographic findings return to normal after 2 days to 2 wks, with an average resolution time of 1 week (3). Our study is concordant with previously reported sequential changes.

In this study, GGO, consolidation, and nodules tended to be observed mainly in the subpleural lungs, and GGO and consolidation were distributed in the lower part of the lung, while the nodule was distributed in the upper part of the lung, but these observations were not statistically different. Previous studies showed that the pathology of PFE tended to be localized with various distributions, which was probably due to the irregular distribution of the fat embolization (19, 22). According to Arakawa et al. (15), the CT findings of PFE were predominantly found in the upper lobes of the lungs. Another report showed the tendency to be distributed in the lower lungs and this was explained by the hemodynamics such as the distribution of the blood flow through the inferior vena cava into the lower lobes (21). However, in this study, the fat was introduced from the ear vein through the superior vena cava; thus, this may become one reason to be different from the distribution of PFE observed in humans after a long bone fracture or a soft tissue injury.

There were a few limitations in this study. First, experimental pulmonary fat embolism is induced by use of linoleic acid, which has been not used in previous studies. However, the decision to use it was made after sufficient consideration in the pilot study. Second, the number of experimental subjects was too small to represent CT findings according to a time course and according to the changes in the pathologic findings. Third, the classical diagnosis of PFE follows the major and supplementary diagnostic criteria of the clinical symptoms and the laboratory findings (23). According to these criteria, it was not clear whether or not PFE was artificially induced in the experiment. However, it was histopathologically proved that the occlusion of the pulmonary vessels and the alveolar inflammation were caused by fat embolism. Thus, this study is considered to be useful for the investigation of the CT findings of PFE and for the related studies on the histopathological findings.

In conclusion, PFE was caused by using linoleic acid, which is kind of FFA, in all rabbits and as for our study, presentation can become one model of the occurrence of nontraumatic PFE. CT accurately depicted the natural evolution of the pulmonary fat embolism on serial follow-up, and this correlated well with the pathologic findings. Furthermore, changes of lung parenchyma by the toxicity of free fatty acid could serve as the basic data for not only studies on the mechanical theory, but also for studies on the biochemical theory and on the pathogenesis of PFE.

Experimental pulmonary fat embolism was induced by free fatty acids and CT findings were observed over the course of time. In many cases, it is difficult to discern abnormal CT findings of patients with no clinical trauma (14) or mild trauma, and consequently, it is easy to overlook pulmonary fat embolism. This study may explain possibilities of diseases observed by patients by understanding the natural courses and CT findings of pulmonary fat embolism; and may suggest good prognoses. Furthermore, based on the findings of the experiment, broader studies on pulmonary fat embolism will be possible.

REFERENCES

1. Moylan JA, Birnbaum M, Katz A, Everson MA. *Fat emboli syndrome. J Trauma 1976; 16: 341-7.*
2. Dines DE, Burgher LW, Okazaki H. *The clinical and pathologic correlation of fat embolism syndrome. Mayo Clin Proc 1975; 50: 407-11.*
3. Batra P. *The fat embolism syndrome. J Thorac Imaging 1987; 2: 12-7.*
4. Shier MR, Wilson RF. *Fat embolism syndrome: traumatic coagulopathy with respiratory distress. Surg Annu 1980; 12: 139-68.*
5. Baker PL, Pazell JA, Peltier LF. *Free fatty acids, catecholamines, and arterial hypoxia in patients with fat embolism. J Trauma 1971; 11: 1026-30.*
6. Burhop KE, Selig WM, Beeler DA, Malik AB. *Effect of heparin on increased pulmonary microvascular permeability after bone marrow embolism in awake sheep. Am Rev Respir Dis 1987; 136: 134-41.*
7. Byrick RJ, Wong PY, Mullen JB, Wigglesworth DF. *Ibuprofen pretreatment does not prevent hemodynamic instability after cemented arthroplasty in dogs. Anesth Analg 1992; 75: 515-22.*
8. Nakata Y, Tanaka H, Kuwagata Y, Yoshioka T, Sugimoto H. *Triolein-induced pulmonary embolization and increased microvascular permeability in isolated perfused rat lungs. J Trauma 1999; 47: 111-9.*
9. Nakata Y, Dahms TE. *Triolein increases microvascular permeability in isolated perfused rabbit lungs: role of neutrophils. J Trauma 2000; 49: 320-6.*

10. Byrick RJ, Kay JC, Mullen JB. *Pulmonary marrow embolism: a dog model simulating dual component cemented arthroplasty*. *Can J Anaesth 1987; 34: 336-42*.
11. Baker PL, Kuenzig MC, Peltier LF. *Experimental fat embolism in dogs*. *J Trauma 1969; 9: 577-86*.
12. Gossling HR, Pellegrini VD Jr. *Fat embolism syndrome: a review of the pathophysiology and physiological basis of treatment*. *Clin Orthop Relat Res 1982; 68-82*.
13. Szabo G. *The syndrome of fat embolism and its origin*. *J Clin Pathol Suppl (R Coll Patho) 1970; 4: 123-31*.
14. Choi JA, Oh YW, Kim HK, Kang KH, Choi YH, Kang EY. *Nontraumatic pulmonary fat embolism syndrome: radiologic and pathologic correlations*. *J Thorac Imaging 2002; 17: 167-9*.
15. Arakawa H, Kurihara Y, Nakajima Y. *Pulmonary fat embolism syndrome: CT findings in six patients*. *J Comput Assist Tomogr 2000; 24: 24-9*.
16. Malagari K, Economopoulos N, Stoupis C, Daniil Z, Papiris S, Muller NL, Kelekis D. *High-resolution CT findings in mild pulmonary fat embolism*. *Chest 2003; 123: 1196-201*.
17. Derks CM, Jacobovitz-Derks D. *Embolic pneumopathy induced by oleic acid*. *A systematic morphologic study*. *Am J Pathol 1977; 87: 143-58*.
18. Park SJ, Sung DW, Jun YH, Oh JH, Ko YT, Lee JH, Yoon Y. *Pulmonary fat embolism induced intravenous injection of autologous bone marrow in rabbit: CT and pathologic correlation*. *J Korean Radiol Soc 1999; 41: 303-11*.
19. Berrigan TJ Jr, Carsky EW, Heitzman ER. *Fat embolism*. *Roentgenographic pathologic correlation in 3 cases*. *Am J Roentgenol Radium Ther Nucl Med 1966; 96: 967-71*.
20. King EG, Wagner WW Jr, Ashbaugh DG, Latham LP, Halsey DR. *Alterations in pulmonary microanatomy after fat embolism*. *In vivo observations via thoracic window of the oleic acid-embolized canine lung*. *Chest 1971; 59: 524-30*.
21. Muangman N, Stern EJ, Bulger EM, Jurkovich GJ, Mann FA. *Chest radiographic evolution in fat embolism syndrome*. *J Med Assoc Thai 2005; 88: 1854-60*.
22. Feldman F, Ellis K, Green WM. *The fat embolism syndrome*. *Radiology 1975; 114: 535-42*.
23. Gurd AR. *Fat embolism: an aid to diagnosis*. *J Bone Joint Surg Br 1970; 52: 732-7*.